Search for long-lived 2S muonic hydrogen in H_2 gas

P. O. Egan, S. Dhawan, V. W. Hughes, D. C. Lu, F. G. Mariam, P. A. Souder, and J. Vetter
J. W. Gibbs Laboratory, Yale University, New Haven, Connecticut 06520

G. zu Putlitz
Physikalisches Institut, Universität Heidelberg, D6900 Heidelberg, Federal Republic of Germany

P. A. Thompson*
Los Alamos Scientific Laboratory, Los Alamos, New Mexico 87545

A. B. Denison
Physics Department, University of Wyoming, Laramie, Wyoming 82071
(Received 18 July 1980)

We have searched for long-lived 2S muonic hydrogen ($\mu^- p$) in H_2 gas at 0.8 atm. The state could be detected by observing delayed 1.9-keV $2P \rightarrow 1S$ photons from collisionally quenched $\mu^- p(2S)$. The observed upper limit (90% confidence level) for the fraction, f_{2S}, of $\mu^- p(2S)$ with lifetime τ_{2S} in the gas in the range, $100 < \tau_{2S} < 1000$ ns, is $f_{2S} < 2\%$. Our results are consistent with the view that most of the $\mu^- p(2S)$ have kinetic energies greater than the 0.3-eV threshold for the inelastic collision $\mu^- p(2S) + H_2 \rightarrow \mu^- p(2P) + H_2$ and hence are rapidly quenched. We have also measured the relative Lyman line intensities in muonic hydrogen and muonic helium at 0.8 atm with solid-state detectors [Ge for $\mu^- {}^4He$ and Si(Li) for $\mu^- p$]. The results are $(K_\alpha / K_{\text{total}})_{\mu - p} = 0.46 \pm 0.06$, $K_\alpha / K_{\text{total}})_{\mu - {}^4He} = 0.76 \pm 0.04$, $(K_\beta / K_{\text{total}})_{\mu - {}^4He} = 0.04 \pm 0.02$. These results imply that about 7.5% of $\mu^- p$ atoms cascade to the 2S state.

I. INTRODUCTION

Muonic hydrogen is the atom consisting of a negative muon and a proton. Table I lists some basic properties of $\mu^- p$, compared to hydrogen ($e^- p$). The energy levels for the $n=1$ and $n=2$ states of $\mu^- p$ have been calculated[1-4] and are shown in Fig. 1.

A principal interest in $\mu^- p$ at present is the possibility of measuring the fine structure, Lamb shift, and hyperfine structure intervals of the $n=2$ state in a laser spectroscopy experiment similar to that in which the fine structure of the $n=2$ state of $\mu^- {}^4He$ was measured.[5] Such measurements would provide an important test of muon electrodynamics as well as information about proton structure.[6-8] This experiment would require atoms in the metastable 2S state, and we report here experimental studies of the formation and lifetime of $\mu^- p$ in the 2S state in H_2 gas.

TABLE I. Basic properties of muonic hydrogen and hydrogen.

	Muonic hydrogen ($\mu^- p$)	Hydrogen (H)
Mass	1044.0 MeV	938.8 MeV
Reduced mass	95.0 MeV	0.511 MeV
Rydberg energy	2.53 keV	13.6 eV
Bohr radius	2.8×10^{-11} cm	5.3×10^{-9} cm
Radiative rates	186 λ_H	λ_H

The characteristics of the $n=2$ state of $\mu^- p$ are of particular relevance to the present paper. The metastable $2^2S_{1/2}$ level lies below the $2^2P_{1/2}$ level by 0.2 eV, which is determined principally by the dominant electron vacuum polarization term. The transition energy from the 2P to the 1S state is 1.9 keV, and the spontaneous decay rate for $2P \rightarrow 1S$ is $\lambda(2P \rightarrow 1S) = 1.3 \times 10^{11}$ s^{-1} (Ref. 9). The dominant spontaneous decay of the 2S state is a

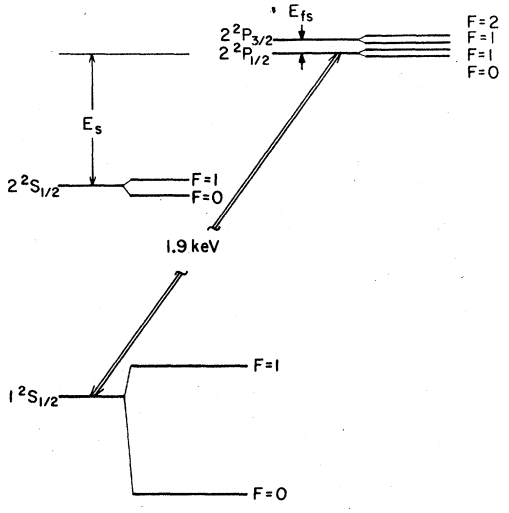

FIG. 1. Energy level diagram of muonic hydrogen in the $n=1$ and $n=2$ states. The $2^2S_{1/2} - 2^2P_{1/2}$ interval E_S is 0.20 eV and the $2^2P_{1/2} - 2^2P_{3/2}$ fine structure interval, E_{fs} is 0.008 eV. The hfs interval in the $n=1$ state is 0.18 eV.

 © 1981 The American Physical Society

TABLE II. Mechanisms involved in deexcitation of muonic hydrogen.

Chemical reaction	$(\mu^- p)_{n_i} + H_2 \rightarrow (\mu^- p)_{n_f} + 2H + KE$
Auger effect	$(\mu^- p)_{n_i} + H_2 \rightarrow (\mu^- p)_{n_f} + H_2^+ + e^-$
Stark mixing (nonradiative) (or Coulomb deexcitation)	$(\mu^- p)_{n_i} + H_2 \rightarrow (\mu^- p)_{n_f} + H_2 + KE$
Stark mixing (radiative)	$(\mu^- p)_{n_i l_i} + H_2 \rightarrow (\mu^- p)_{n_i l'} + H_2$ $\hookrightarrow (\mu^- p)_{n_f, l' \pm 1} + \gamma$
Radiative transition	$(\mu^- p)_{n_i l_i} \rightarrow (\mu^- p)_{n_f l_i \pm 1} + \gamma$

two-photon transition[10] with decay rate $\lambda(2S \rightarrow 1S) = 1.7 \times 10^3\ s^{-1}$, which is slow compared to the free muon decay rate $\lambda_\mu = 4.5 \times 10^5\ s^{-1}$.

The formation and deexcitation of $\mu^- p$ have been treated theoretically by various authors.[11-14] Briefly, a low-velocity muon is captured by H_2 into a highly excited muonic orbital $[n \gtrsim (m_\mu/m_e)^{1/2} \sim 14]$ followed by a breakup of the hydrogen molecule. The $\mu^- p$ quickly cascades to the ground state or the 2S state through the mechanisms listed in Table II. The various deexcitation mechanisms depend on gas density as well as on the quantum numbers (n,l) for a muonic state. In low-density gases, the Stark mixing is particularly important as the atom deexcites to values of n below 14, where the $\mu^- p$ Bohr radius is smaller than the sizes of molecules. The neutral $\mu^- p$ atom can then penetrate close to the nuclei of the gas molecules where it experiences large electric fields. The Stark effect mixes states of different l and therefore decreases the mean radiative lifetime of the Bohr levels and increases the probability that atoms are in sublevels of low l. In particular, the mixing increases the chance of $P \rightarrow S$ transitions leading to an increase of the yield of 2S atoms. Ultimately, most of the atoms will arrive in the ground 1S state, while some fraction (1 to 8%, depending on the magnitude of the Stark mixing) will populate the 2S level.

The most important quenching of $\mu^- p(2S)$ will involve the near-lying 2P state and depends critically on whether the kinetic energy of the atom is above the threshold energy for excitation to the 2P state in a collision with an H_2 molecule. This threshold kinetic energy in the laboratory frame of reference is about 0.3 eV corresponding to the 0.2-eV energy difference between the $2\,^2P_{1/2}$ and $2\,^2S_{1/2}$ states. If collisional excitation to the 2P state occurs, it will be followed by radiative decay to the 1S state. The cross section for deexcitation of the 2S state by this process has been calculated[15,16] to be $\approx 10^{-16}$ cm^2 for relative kinetic energies of 1 eV. At pressures of 1 atm this cross section results in a lifetime of the 2S state, $\tau_{2S} \approx 10^{-10}$ s.

If the relative kinetic energy of the atom is below the 0.31-eV threshold, the inelastic channel is closed, and quenching of the 2S state can only occur by Stark mixing of the 2S and 2P states during the collision, accompanied by radiative decay of the P admixture. The cross sections below threshold have been calculated using a quantum mechanical approach in the adiabatic approximation.[17] The results of the calculations yield quenching cross sections of $\sim 2 \times 10^{-19}$ cm^2 for kinetic energies below theshold. The corresponding 2S lifetime in 1-atm H_2 is a few hundred nanoseconds. For example, at a kinetic energy of 0.1 eV the theory predicts, $\tau_{2S} \simeq (400/P)$ ns, where P is the H_2 pressure in atmospheres (at 0 °C).

The velocity distribution of the $\mu^- p$ depends on the complex series of atomic and molecular processes determining the deexcitation (Table II). In particular, the chemical deexcitation process is exothermic with 4.5 eV available from the dissociation of the H_2 molecule. The radiationless Stark deexcitation is also able to impart energies of the order of a few electron volts to the system.[18] Experimental studies of the diffusion of $\mu^- p(1S)$ (Refs. 19 and 20) indicate kinetic energies in the range 0.1–1.0 eV but are rather imprecise. Although it can be expected that the kinetic energies of $\mu^- p(1S)$ and $\mu^- p(2S)$ atoms will be nearly the same, still there is no direct experimental information on the kinetic energies of $\mu^- p(2S)$ atoms.

Our experiment was done at the Los Alamos Meson Physics Facility (LAMPF) and is designed principally to observe delayed 1.9-keV x rays which would arise from the collisional quenching of $\mu^- p(2S)$ in the time interval from 50 ns to 1.0 μs after the μ^- stops in the H_2 gas. A similar experiment has recently been reported from the Swiss Institute for Nuclear Research (SIN).[21,22] No appreciable number of delayed x rays with energies near 1.9 keV will arise from the spontaneous two-photon decay of $\mu^- p$ atoms in the 2S state because

of the relatively slow two-photon decay rate and because of the continuous energy spectrum of this decay mode.

In an additional phase of our experiment we measured the relative intensities of the Lyman transitions in both muonic hydrogen and the muonic helium ion $(\mu^{-4}\mathrm{He})^+$ at atmospheric gas densities, using solid-state photon detectors. The relative intensities of the Lyman lines are important because they reflect the different processes involved in the de-excitation of the muonic atom from its initial highly excited state. The measurement of the $(K_\alpha/K_{\text{total}})_{\mu^- p}$ ratio determines the fraction of $\mu^- p$ atoms which cascade to the 2S state.

The muonic hydrogen Lyman transitions were first observed by Placci *et al.*[23] at H_2 densities of 4 atm. The transitions have also been seen in liquid H_2 (Ref. 24). The only previous measurement of $(\mu^{-4}\mathrm{He})^+$ intensities in gases[25] was made in 7-atm helium and used a proportional chamber to measure the x-ray energy. Solid-state detectors have previously been used to observe the $(\mu^{-4}\mathrm{He})^+$ transitions in liquid helium.[26,27] For muonic hydrogen the measurements of Lyman transitions have all utilized proportional chambers.[21,23,24]

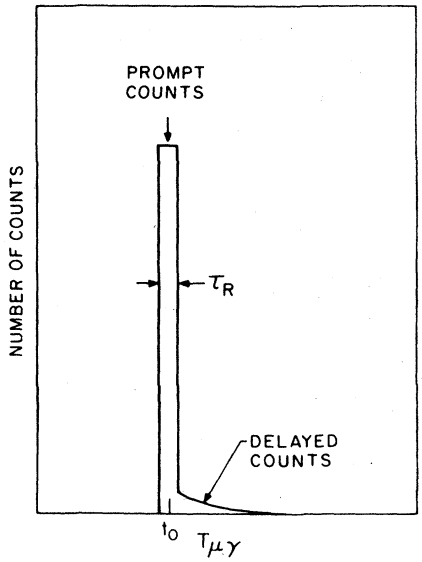

FIG. 2. Idealized view of the expected time distribution of $\mu^- p$ Lyman photons. $T_{\mu\gamma}$ is the time between a muon stop in the target and a photon event. The shape of the prompt peak is due to the time resolution of the detector, τ_R. The delayed spectrum shown is 5% of the prompt peak with decay time $\tau_{2S} = \tau_R$.

II. EXPERIMENTAL TECHNIQUE

The method of looking for delayed $\mu^- p(2P \to 1S)$ 1.9-keV x rays to determine the long-lived fraction of $\mu^- p(2S)$ is straightforward. The $\mu^- p$ atoms are formed by stopping μ^- in an H_2 target, and a logic signal is derived from beam counters which determines the time t_0 when the muon stops in the H_2 target and forms $\mu^- p(2S)$. Detectors sensitive to the 1.9-keV Lyman radiation determine the energy and time of emission of x rays with respect to t_0. Figure 2 shows an idealized view of what one might expect. The dominant feature of the spectrum will be the prompt Lyman radiation from the P states. Any Lyman $(nP \to 1S)$ photons from collisionally quenched metastable 2S states could be detected a few hundred nanoseconds after t_0 with a characteristic lifetime τ_{2S}.

A. Target and counter assembly

Figure 3 shows a simplified layout of the experimental apparatus. The LAMPF stopped muon channel[28] is tuned to produce μ^- at 47 MeV/c, to optimize the stopping width in the thin (~3 mg cm^{-2})

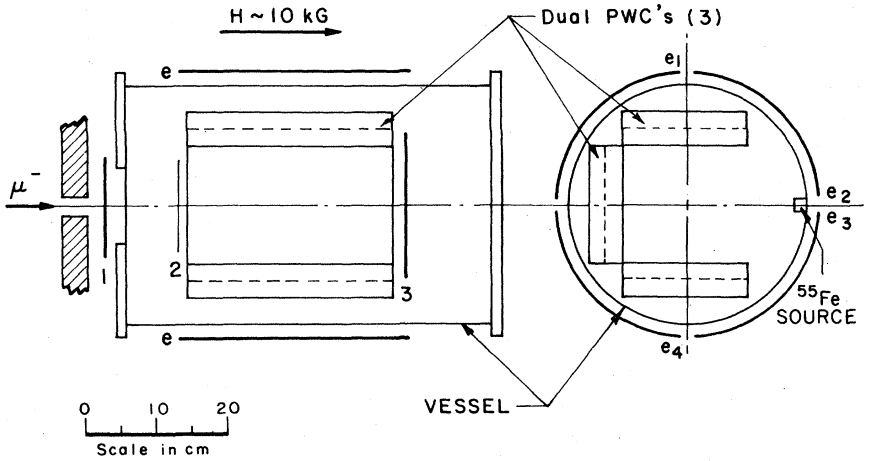

FIG. 3. Diagram of the experimental apparatus. 1, 2, 3, and e_i are plastic scintillation counters.

gas target. Stopping muons are signaled in plastic (NE110) scintillation counters 1, 2, and 3. Counters 2 and 3 are located inside the gas vessel. Counter 2 is extremely thin, 0.13 mm, to minimize false events from muons stopping in the counter. Light is coupled from this scintillator to an outer lucite annulus, 0.16-cm thick, and is viewed by two RCA 8850 photomultiplier tubes (PMT). Counters 1 and 3 are 0.16 and 0.32 cm thick respectively. Both internal counters are wrapped with a single layer of 6-μm aluminized Mylar to reduce cross talk and increase light collection efficiency, and the light is led out of the vessel by lucite light pipes and quartz windows in the end flanges. Counter 2, the thin scintillator, was observed to yield roughly 3–4 photoelectrons in the PMT for an entering muon.

A muon stopping in the active region of the target gas or in counter 2, is signaled by $\mu_S = 12\bar{3}$. At 47 MeV/c we obtained average μ_S rates as high as 3×10^3 s^{-1}, of which approximately 10% are stops in the gas. During the actual data acquisition these rates were lowered a factor of 10 by collimation to reduce the entering muon rate in counter 1 and ensure that only one muon at a time is in the stopping region.

In addition to the stopping counters, the outer diameter of the gas vessel was surrounded by 0.64-cm-thick scintillators, $e1$–$e4$. These counters were used to detect the decay electron from the stopping muon under observation to ensure that the signals observed by the photon detectors are not associated with muon decay.

The gas vessel for the experiment was a stainless-steel cylinder of 33-cm diameter and 3-mm wall thickness. The end plates of the vessel were 1.0-cm-thick stainless steel and the upstream end plate had a 10-cm-diameter entrance aperture for the muon beam, covered by a 0.1-mm stainless-steel window. All feedthroughs for light guides, gas, and electronics were made through the end plates.

The hydrogen gas for the experiment was ultra high purity (99.999% H_2) and was continuously flowed through the vessel at ~10 liter/hr. After initial pumpout and filling, the gas pressure was maintained at ~1 Torr above the local atmospheric pressure (600 Torr at Los Alamos), and the pressure was monitored by a quartz bourdon tube gauge. Periodic samples of the outlet gas were analyzed by mass spectroscopy.

The photon detectors for the experiment were gas proportional chambers with multiwire anodes and cathodes (MPWC's). The design of the chambers is shown in Fig. 4. The thin window separating the counter gas from the H_2 stopping gas is 6-μm aluminized Mylar, mounted flush

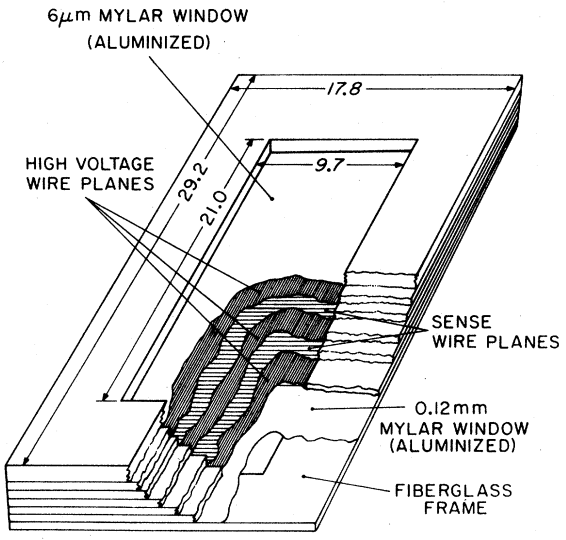

FIG. 4. Diagram of the proportional wire chambers. Dimensions in cm.

against the first HV plane. Each wire plane is strung on a G-10 fiberglass frame 6.3-mm thick. The chambers consist of two planes of sense wires and three HV planes with plane-to-plane gap of 6.3 mm. The spacing of the 20-μm diameter sense wires is 3 mm, while the 50-μm HV wires are spaced 1.5 mm apart and strung perpendicular to the sense wires. The 64 sense wires of each plane are connected in parallel to printed circuits on the frame. The induced pulses were amplified by a charge sensitive preamp mounted directly on the chamber. The output signal for the 5.9-keV ^{55}Fe line was 1 volt into 50 Ω at a chamber high voltage of 2300 V. The theoretical efficiency for 1.9-keV photons, with P-10 counter gas (90% Ar, 10% CH_4) is 42% for a single plane and 59% for two planes. Three of the PWC units were mounted inside the H_2 vessel with entrance window 10 cm from the beam axis. Typical operating voltages on the cathodes were 2200–2400 V with P-10 gas.

Tests of the chambers with standard x-ray sources indicated a fractional energy resolution of 17–23% for the Mn K x ray (6.0 keV) and time resolution of ~300 ns for the Cu K x ray (8.1 keV). The time jitter is determined by the drift time difference of the ionization electrons in the chamber. An ^{55}Fe source inside the target vessel allows calibration during the experiment.

The entire apparatus is positioned at the center of a large high-precision solenoid magnet.[29] The magnetic field of 10 kG is directed along the beam axis and confines the muon stopping distribution to the axis. Previous measurements of muon stopping distributions inside this magnet had shown

the radial stopping distribution to be Gaussian with $\sigma = 2$ cm.

B. Electronics and data acquisition

Figure 5 is a simplified schematic diagram of the electronic logic for the experiment. A muon incident on the apparatus is detected in counter 1 and denoted μ_I. A muon stopping in the observation region of the H_2 gas or in counter 2, μ_S, is signaled by a coincidence $12\bar{3}$.

If the PWC's were insensitive to the electron background from muons stopping in the inactive regions of the apparatus, we could use the full beam intensity and have a rate of $\sim 10^3$ μ_S per second. Unfortunately, the PWC's are sensitive to electrons, and a minimum ionizing e^- deposits ~2 keV in the chamber, so that delayed electrons from muon decay could easily be misidentified as Lyman photons. To avoid this difficulty we require that there shall not be a μ_I in the 4 μs preceding a μ_S, nor a μ_I in the 4 μs after a μ_S. The suitably blocked signal is called TRIGGER in the diagram. We also require that in addition to observing a photon event (γ) from the stopped muon, we must also see an electron event (e) in the external electron counters, e_1–e_4.

To meet the blocking requirements on entering muons with the 6% LAMPF duty factor, the beam was collimated to 5 cm^2 and the instantaneous μ_I rate was reduced to 7×10^4 s^{-1} (5×10^3 s^{-1} average), which brought the average μ_S rate to ~320 s^{-1}, of which ~30 s^{-1} were stops in the gas.

The proportional wire chamber signals from the internal charge sensitive preamps went to amplifiers (Tennelec 205A). The fast bipolar outputs were discriminated and a logic signal was derived when there was a count in an inner or A plane and no count in any outer or B plane. This signal (γ) was used to gate a peak-sensing CAMAC ADC (LRS 2259A). The three ADC inputs were the slow unipolar outputs (shaping constant 0.25 μs) from the PWC amplifiers for the A planes. The pulse heights, E1, E2, E3, of the PWC outputs were read by computer interrupt whenever the ADC signaled that there were data available.

The logical coincidence between a suitably delayed γ and the TRIGGER gate is denoted γ_μ and signals a good event. The ADC conversion started by the γ signal can be cleared and the event rejected if any of the following occur.

(a) No electron (e) is seen in a 3-μs gate following the γ_μ, i.e., we must see the decay electron.

(b) A second μ_I occurs within 4 μs after the μ_S.

(c) No TRIGGER gate accompanies the γ, i.e., no γ_μ.

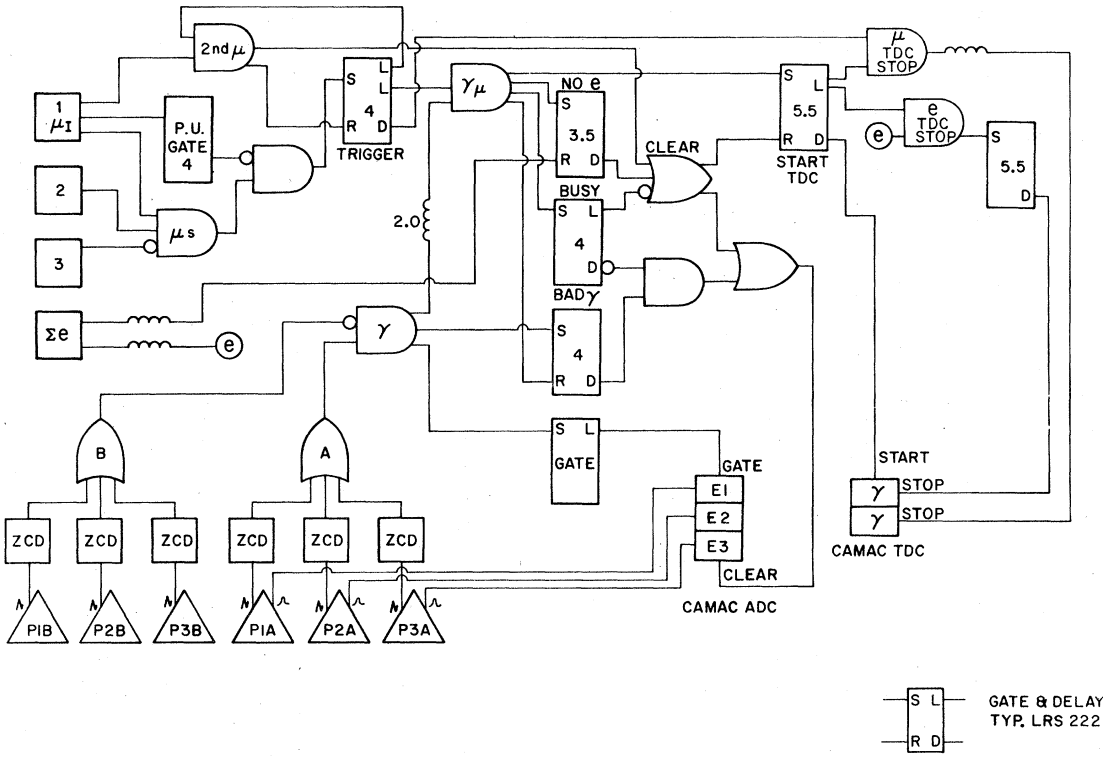

FIG. 5. Simplified schematic diagram of the electronic logic. P1A and B denote the charge sensitive preamps for PWC 1 inner (A) and outer (B) plane. ZCD= zero crossing discriminator. All times are in microseconds.

(d) A second γ occurs within 4 μs.

The time information is obtained by using a CAMAC TDC (LRS 2226 modified so full scale is 4.0 μ_S). The START pulse for the TDC comes from a suitably delayed γ_μ. One channel of the TDC is stopped by a TRIGGER, while the other channel is stopped by an e. The TDC thus records $T_{\gamma e}$ the time difference between a photon event and an electron event, as well as $T_{\mu\gamma}$ the time difference between a muon stop in the gas and a photon. The TDC is read along with the ADC and all data are written on magnetic tape and histogrammed in the computer memory. In addition to the time and energy information, scaler rates for all logic signals are recorded by the computer.

III. ANALYSIS AND RESULTS

The information, E_1, E_2, E_3, $T_{\mu\gamma}$, $T_{\gamma e}$, for each event is recorded on magnetic tape, so the experiment can be analyzed with different cuts on these parameters.

A. $T_{\gamma e}$ spectrum

The first aspect of the analysis was ensuring that photons detected in the PWC were not associated with decay electrons. Thus we determined the $T_{\gamma e}$ distribution, that is, the time between the arrival of a photon and a decay electron. Figure 6 shows a plot of this spectrum for all PWC's, for two different cuts on the photon energy E. In Fig. 6(a) all values of the pulse height are included, and in Fig. 6(b) only events with photon energy within the half-width of the Lyman spectrum (as determined below) are accepted. The large spike at t_0 is due to γ's coincident with the muon decay, either decay bremsstrahlung or decay electrons misidentified as photons. The counts occuring after t_0 are the events of interest, i.e., a photon followed by a muon decay. In the subsequent analysis we therefore accept only events with $T_{\gamma e} > t_c$, where t_c is a value which is greater than the prompt spike. Varying the choice of t_c had no significant effect on the analysis. This procedure gives a clean sample of photons not associated with decay electrons.

The $T_{\gamma e}$ counts for times before t_0 indicate that the muon blocking logic is not completely effective, which is to be expected since the blocking time is rather short (4 μs) and a good fraction of muons in the target region live longer than this. The counts before t_0 are then due to an electron count from a senile muon in the target together with a "photon" count (γ). Indeed, in this case most of the photon counts do not occur within the Lyman peak and are probably misidentified electrons.

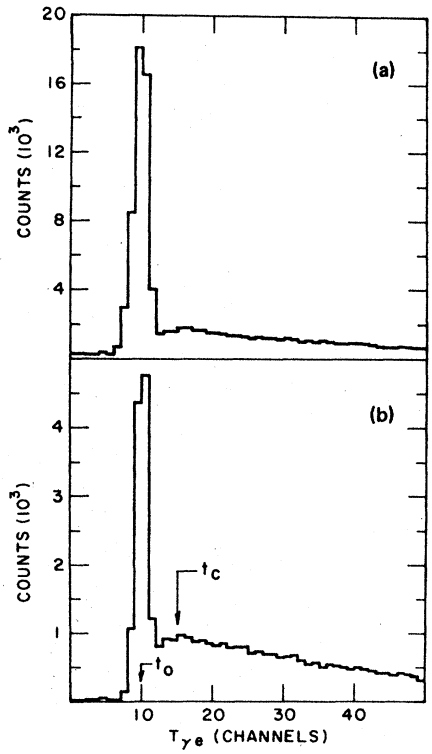

FIG. 6. (a) Spectrum for $T_{\gamma e}$, time between a photon and a decay electron, 1 channel = 64 ns; (b) Same spectrum with requirement that the photon be within FWHM of the Lyman peak. The analysis required that $T_{\gamma e} > t_c$.

Of course, counts due to senile muon decay, muons living longer than the 4-μs blocking gate, are also present in the "good" portion of the spectrum after t_c and will appear as background. We can get an estimate of the magnitude of this effect by comparing the count rate before t_c, R (senile μ), with the rate after t_c, R(good), and we find

$$\frac{R(\text{senile } \mu)}{R(\text{good})} = 0.017 \pm 0.001 . \quad (1)$$

The shape of the $T_{\gamma e}$ spectrum for times greater than t_0 is determined largely by the exponential decay of the muon. Since these counts are due overwhelmingly to muons in the muonic hydrogen atom, the decay spectrum allows an additional test of the gas purity of our target. The transfer of the muon in $\mu^- p$ to an impurity gas atom (for example, Ar from the PWC), is followed by μ capture. For an argon concentration c_{Ar} in our target, the transfer rate to the argon is[30] $\lambda_{Ar}^T = 0.7 \times 10^8 \, c_{Ar}$. The measured decay rate of the muon in $\mu^- p$ from our $T_{\gamma e}$ spectrum is, $\lambda = 4.40(11) \times 10^5 \, s^{-1}$, which agrees with the value for free muon decay and implies that the argon impurities in the target gas have a concentration $c_{Ar} < 2 \times 10^{-4}$.

Other possible impurity gases have smaller transfer rates, hence our value for argon is an upper limit. This result agrees with mass spectrometric analysis of the gas sample which found $c_{Ar} < 10^{-3}$.

B. Prompt energy spectrum

The next phase of the data analysis considered the pulse height distribution of counts in the PWC's associated with prompt Lyman decay, including the $T_{\gamma e}$ cut ($T_{\gamma e} > t_c$) described in the previous section. A plot of the prompt Lyman spectrum for all three detectors is shown in Fig. 7. The energy calibration of the detectors comes from the internal ^{55}Fe (6.0-keV Mn x ray) source. The larger uncertainty of the energy for detector 1 is due to a possible rate dependence of this detector spectrum, discovered after the run. All detectors show a prominent Lyman peak, with a center of gravity slightly above the Lyman-α energy. The detector resolutions ($R \equiv$ FWHM/center) are R(PWC1) $\cong 51\%$, R(PWC2) $\cong 53\%$, R(PWC3) $\cong 48\%$ in agreement with the observed 20% resolution at 6 keV. The counts at energies lower than the Lyman peak are probably a result of chamber inefficiencies or "dead spots," although some may also be due to radiation from stopping muons.

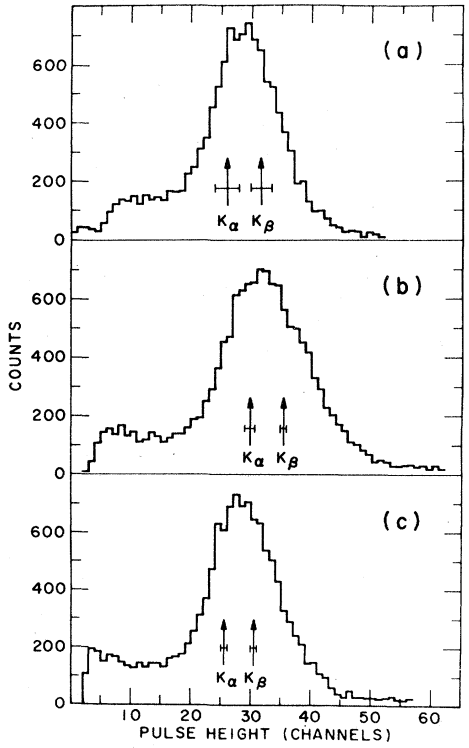

FIG. 7. (a)–(c) Energy spectra for PWC's 1–3. The positions of $K_\alpha = 1.90$ keV and $K_\beta = 2.25$ keV, as determined by the ^{55}Fe calibration of each detector, are shown for each spectrum.

The fact that the line is centered above the Lyman-α energy is due to the fact that a large fraction of the transitions to the ground state occur from states with $n > 2$. The collisional Stark mixing of the higher states leads to a higher probability of P state admixture, and hence a higher $nP \rightarrow 1S$ yield. Theoretical cascade calculations[31,32] including Stark effect predict a Lyman-α yield $K_\alpha/K_{\text{total}} \simeq 0.45$ at 1 atm.

We have fit the energy spectrum for the PWC's with a line shape consisting of two Gaussians, one centered at K_α(1.9 keV) and one with variable energy, K', plus a linear background. The results for the two counters with good calibration are

$$\text{PWC2: } K_\alpha/K_{\text{total}} = 0.49 \pm 0.10,$$
$$K' = 2.37 \pm 0.10 \text{ keV},$$
$$\text{PWC3: } K_\alpha/K_{\text{total}} = 0.55 \pm 0.10,$$
$$K' = 2.33 \pm 0.10 \text{ keV}.$$

In the subsidiary experiment described in Sec. III F of this paper we have measured the Lyman transitions with a solid-state detector and found

$$K_\alpha/K_{\text{total}} = 0.46 \pm 0.06. \quad (2)$$

The $K_\alpha/K_{\text{total}}$ yield is important because it is correlated with the fraction of $\mu^- p$ which cascade to the $2S$ state, ϵ_{2S}. The Stark mixing can increase the $2S$ yield by enhancing transitions $nP \rightarrow 2S$. A theoretical estimate[33] shows that

$$\epsilon_{2S} \cong (1 - K_\alpha/K_{\text{total}})/(7.2 \pm 0.4). \quad (3)$$

Hence the $K_\alpha/K_{\text{total}}$ measurement determines ϵ_{2S}. Using the value of Eq. (2) we find,

$$\epsilon_{2S} \cong (7.5 \pm 1.0)\%. \quad (4)$$

C. $T_{\mu\gamma}$ spectrum

The most important part of the analysis involves the spectrum of $T_{\mu\gamma}$, the time difference between the muon stop and the photon, where delayed x rays from the collisionally quenched $2S$ state could be observed. A plot of the $T_{\mu\gamma}$ spectrum is shown in Fig. 8 with the cut $T_{\gamma e} > t_c$ and the requirement that the γ energy lies within the half-width of the Lyman peak (Fig. 7). The prompt Lyman peak dominates the spectrum, and the shape of this peak is determined by the time resolution function of the PWC's. The resolution function is seen to be a rectangular pulse shape with FWHM = 270 ns, and steep sides, rising from 10 to 90% in 40 ns. This shape agrees with that determined in earlier calibrations with x-ray sources.

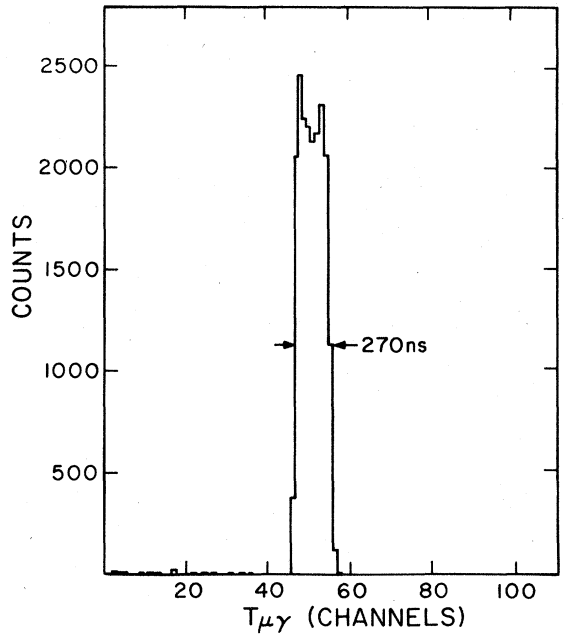

FIG. 8. Time spectrum for $T_{\mu\gamma}$, time between Lyman photon and muon stop. The events outside the prompt peak are barely visible on this scale. 1 channel=32 ns.

Although not easily visible in the linear histogram, there are events both before and after the prompt peak. These counts are apparent in the logarithmic plot of $T_{\mu\gamma}$ of Fig. 9. The notch for times immediately prior to the prompt spike is visible in the spectrum without the $T_{\gamma e}$ cut and presumably is due to the B plane veto of the PWC's, that is, senile decay electrons misidentified as γ's are in turn vetoed by B plane counts associated with the μ stop.

The numbers of counts for the three regions of the spectrum are

$N_{\text{prompt}} = 23\,205$ counts in 300 ns,

$N_{\text{delayed}} = 145$ counts in 1.63 μs,

$N_{\text{early}} = 517$ counts in 1.13 μs.

We note that the fraction of events after the prompt peak is in rough agreement with the background estimate of Eq. (1). Fitting the $T_{\mu\gamma}$ spectra for the regions before and after the prompt peak to a single exponential decay function yields the lifetimes

$$\tau = 2.5(7) \times 10^{-6}\ \text{s}\,(T_{\mu\gamma}\text{"early"}),$$
$$\tau = 3.0(1.0) \times 10^{-6}\ \text{s}\,(T_{\mu\gamma}\ \text{"delayed"}). \tag{5}$$

These lifetimes are consistent with free muon decay and suggest that the events outside the prompt peak are background counts due predominantly to the decay of senile muons which have lived longer than the 4-μs blocking time.

In order to analyze the data for a component of delayed x rays arising from the collisionally quenched 2S state, we assume there is an initial $\mu^- p(2S)$ population N_{2S}^0 which decays with a lifetime τ_{2S}, giving the intrinsic time spectrum

$$\frac{dN}{dt} = \frac{N_{2S}^0}{\tau_{2S}} e^{-t/\tau_{2S}}, \tag{6}$$

The observed spectrum will be determined by the intrinsic spectrum of Eq. (6) together with the time resolution function of the PWC's which we take to be a unit pulse of width τ_R, and hence has the form

$$\frac{dN}{dt} = \begin{cases} \frac{N_{2S}^0}{\tau_R}(1 - e^{-t/\tau_{2S}}), & t < \tau_R \quad (7a) \\ \frac{N_{2S}^0}{\tau_R}(e^{-t/\tau_{2S}})(e^{\tau_R/\tau_{2S}} - 1), & t > \tau_R. \quad (7b) \end{cases}$$

The smearing of the exponential means that we can see decay events for $\tau_{2S} < \tau_R$ in spite of the presence of the prompt peak.

We determined the fraction of the delayed $T_{\mu\gamma}$ spectrum due to an exponential of the form, Eq. (7b) with $\tau_R = 270$ ns (see Fig. 8). The delayed spectrum was fit to two exponentials,

$$F(t) = N_1 e^{-t/\tau} + N_2 e^{-t/\tau_{2S}}, \tag{8}$$

where τ_{2S} is fixed and the other parameters are allowed to vary. The fitting procedure used the method of maximum likelihood, with Poisson statistics. This procedure maximizes the log-likelihood function.

$$\omega \equiv \ln L = \sum_i [\, y_i \ln F(t_i) - F(t_i)], \tag{9}$$

where F is the fitting function of Eq. (8) and the

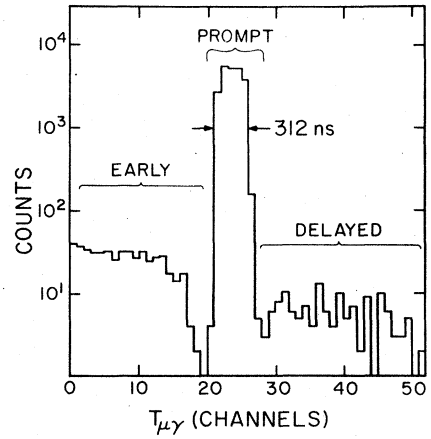

FIG. 9. Logarithmic plot of time spectrum for $T_{\mu\gamma}$, time between Lyman photon and muon stop. 1 channel = 64 ns.

y_i's are the individual data points for times t_i.

For values of τ_{2S} between 50 and 1000 ns the best fits were always obtained for $N_2 = 0$. To determine the sensitivity of this method to N_2, we vary the value of N_2 with the other parameters fixed by the fitting procedure and calculate the log-likelihood, $\omega(N_2)$. The upper limit confidence levels, η, for N_2 can then be determined by calculating the value for which

$$\sum_{i=0}^{N_2} e^{-\omega(i)} \Big/ \sum_{i=0}^{\infty} e^{-\omega(i)} = \eta . \tag{10}$$

The results can then be combined with Eq. (7b) to determine the upper limits for N_{2S}^0.

The results are shown in Fig. 10, where the 90% C.L. upper limits for $N_{2S}^0/N_{\text{prompt}}$ are plotted against τ_{2S}. The plot also shows the limits in terms of f_{2S}, the fraction of the 2S population with lifetime τ_{2S}, where the 2S yield, ϵ_{2S}, is given by Eq. (4). The results put the 90% C.L. upper limits for $N_{2S}^0/N_{\text{prompt}}$ at the level of 1×10^{-3} for $100 < \tau_{2S} < 1000$ ns, and for the metastable fraction f_{2S} below the 2% level. The limits rise quickly for $\tau < 100$ ns reaching $N_{2S}^0/N_{\text{prompt}} = 5 \times 10^{-3}$, $f_{2S} \lesssim 5\%$, for $\tau_{2S} = 50$ ns.

These results can be compared with a recent similar experiment at SIN (Refs. 21 and 22) which searched for the same process at H_2 densities of 600 and 150 Torr. The upper limits determined for f_{2S} (90% C.L.) were

$$f_{2S}(600 \text{ Torr}) \leq 16\%,$$

$$f_{2S}(150 \text{ Torr}) \leq 4\%,$$

where in both cases the τ_{2S} was assumed to be $\tau_{2S} = 400 \text{ ns}/P(\text{atm})$. The SIN work is currently being extended to lower pressures[22] (1–100 Torr).

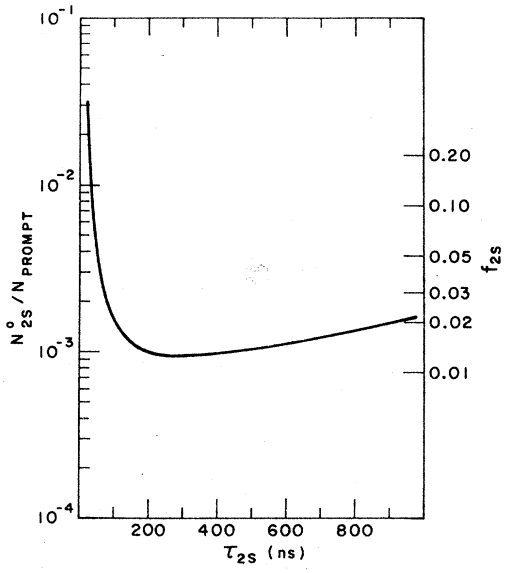

FIG. 10. 90% confidence level upper limits for production of 2S muonic hydrogen with lifetime τ_{2S}. The left scale shows the yield of long lived $\mu^- p(2S)$ as a fraction of the prompt Lyman radiation. The right scale shows fraction of $\mu^- p(2S)$ state which is long lived, assuming the 2S formation fraction ϵ_{2S}, is 7.5%.

D. Delayed energy spectrum

We present the energy spectrum of the delayed $T_{\mu\gamma}$ events in Fig. 11. We have previously identified these events as decay electrons (III C), and the energy spectrum supports this conclusion, since there is no peak at the Lyman energy but rather a broad distribution characteristic of minimum ionizing particles in the PWC.

E. Data with 1% helium admixture

Following the suggestion of Fiorentini and Torelli[34] that small admixtures of He will capture the muon from $\mu^- p(2S)$ but leave $\mu^- p(1S)$ unaffected, we have taken data with 1% He added to the stopping gas. The resulting $T_{\mu\gamma}$ spectrum showed no significant differences from that taken with pure hydrogen.

F. Measurement of $(\mu^- p)$ and $(\mu^- {}^4\text{He})^+$ Lyman intensities with solid-state detectors

In a subsidiary experiment, measurements were made of the intensities of Lyman lines in muonic hydrogen and muonic helium with the experimental set up shown in Fig. 12. The muonic atom was viewed by a solid-state detector mounted in a special Dewar projecting into the gas vessel through the end flange. The detector [Ge or Si(Li)] was 1.0 cm^2 in active area and was mounted 8 mm away from a 25-μm beryllium window which provided the vacuum seal. An additional 8-μm Be

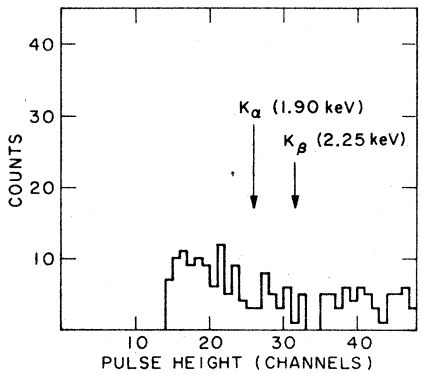

FIG. 11. Energy spectra for delayed $T_{\mu\gamma}$ events, PWC3. The expected positions of the K_α and K_β lines are shown.

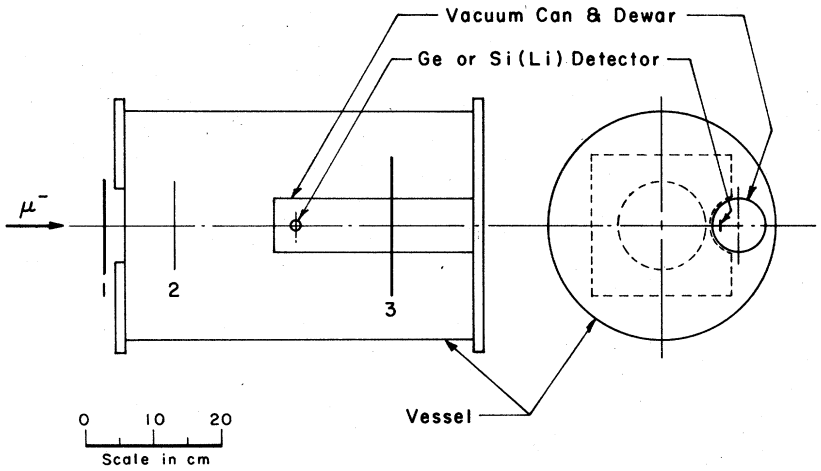

FIG. 12. Diagram of the experimental apparatus to measure muonic hydrogen and muonic helium x rays with solid-state detectors. 1, 2, and 3 are plastic scintillators.

heat shield was placed between the window and the detector. Output pulses from the detector were first amplified in a preamp (optical feedback) and the output signal was split and fed to two amplifiers. One amplifier ($\tau_{\text{shaping}} = 8\ \mu$s) output went to a CAMAC ADC which recorded the pulse height, while the other amplifier provided a timing signal which started a CAMAC TDC to record the time difference between the photon and a muon stop. The energy and time information for each event were stored in a computer and were recorded on magnetic tape. No magnetic field was used in this part of the experiment and the beam collimator was widened to allow μ_S rates of $\sim 10^3\ s^{-1}$.

1. Muonic hydrogen

For muonic hydrogen the observed energy spectrum for events in a 560-ns time window associated with the muon stop is shown in Fig. 13. The energy calibration for the detector was made immediately prior to the run by measuring x-ray fluorescence spectra of Al, Si, P, S, and K. The FWHM of the detector resolution was 280 eV at 2 keV. The $\mu^- p$ spectrum shows a large background with a broad peak at ~5 keV believed due to decay electrons hitting the detector. The smaller hump at 2 keV is due to the prompt Lyman radiation, and is not visible for times delayed with respect to the muon stop, while the electron background still has roughly the same shape.

We have fit the $\mu^- p$ spectrum to two Gaussians with a linear background. The center of the first Gaussian is fixed at the Lyman-α energy while the second Gaussian has variable center E'. The resulting fits gave

$$K_\alpha/K_{\text{total}} = 0.46 \pm 0.06, \qquad (11)$$
$$E' = 2.36 \pm 0.06\ \text{keV},$$

where the efficiencies due to the Be windows, the Si dead layer, and a thin gold layer are all accounted for. These results are compared with other experimental measurements and with the theoretical results of Leon[31] in Table III.

The low intensity of the K_α line is due to strong Stark mixing of the angular momentum substates in the excited states of $\mu^- p$. The result is a dramatic increase in the number of $nP \to 1S$ transitions compared to that predicted for a free atom. As discussed in Sec. III B, this measured value of $K_\alpha/K_{\text{total}}$ determines the fraction of $\mu^- p$ atoms cascading to the 2S state.

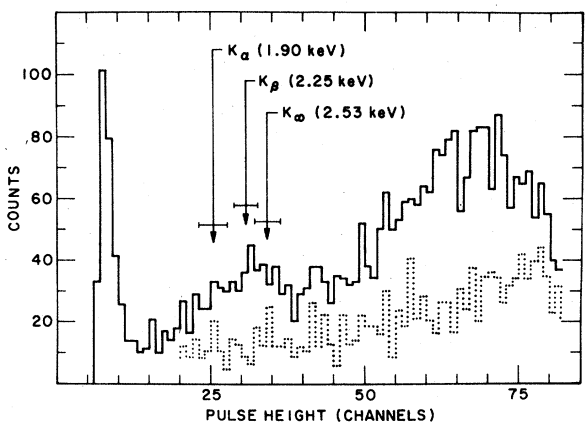

FIG. 13. The solid spectrum shows the pulse-height distribution for $\mu^- p$ in 0.8 atm H_2 for a 560-ns time window associated with a muon stop. Detector: Si(Li). The dotted spectrum shows the background observed for events occurring 1.5 μs after the muon stop. The positions and energies of the Lyman lines, as determined by the x-ray fluorescence calibration, and the resolution of the detector are also indicated.

TABLE III. Summary of muonic hydrogen measurements.

Experiment	Detector	Density	$K_\alpha/K_{\text{total}}$
CERN, 1970 [a]	PWC	4 atm	0.42 ± 0.10
NEVIS, 1971 [b]	PWC	liquid	0.7 ± 0.2
SIN, 1977 [c]	PWC	0.8 atm	0.54 ± 0.08
		0.2 atm	0.53 ± 0.07
This work	Si(Li)	0.8 atm	0.46 ± 0.06
This work	PWC	0.8 atm	0.49 ± 0.10
This work	PWC	0.8 atm	0.55 ± 0.10
Theory [d]		1.0 atm	0.43

[a] Reference 23.
[b] Reference 24.
[c] Reference 21.
[d] Reference 31.

2. *Muonic helium*

Figure 14 shows the Lyman spectrum obtained for muonic helium with a Ge detector within a 250 ns time window associated with a μ stop. The detector calibration was made with a ^{55}Fe (Mn K x-ray) source immediately prior to the run and by observation of the muonic Al M x ray during the run.

The background from decay electrons is again present in the spectrum. The prominent line is the K_α radiation centered at

$$E(K_\alpha) = 8.26 \pm 0.04 \text{ keV}$$

in agreement with the theoretical value[35] of 8.224 keV and the most accurate measurement[27] in liquid He of $E(K_\alpha) = 8.226(2)$ keV.

We observed little, if any, radiation associated with the K_β energy of 9.74 keV. There is, however, a pronounced peak near the end of the Lyman term series ($K_\infty = 10.96$ keV).

The relative intensities of the Lyman transitions are

$$K_\alpha/K_{\text{total}} = 0.76 \pm 0.04\,, \qquad K_\beta/K_{\text{total}} = 0.04 \pm 0.02\,. \tag{12}$$

These ratios are in general agreement with the cascade calculation of Placci *et al.*[25] assuming strong Stark mixing of the l states. A comparison with other measurements is shown in Table IV.

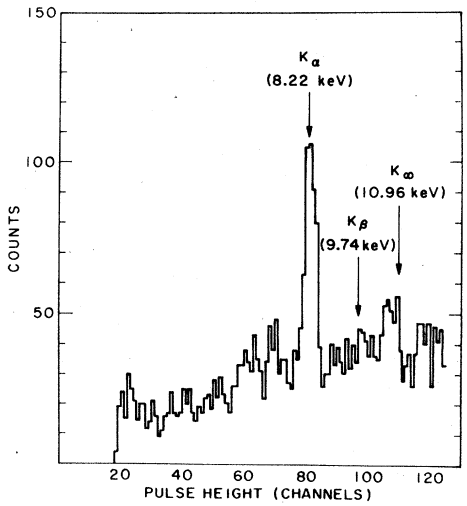

FIG. 14. Pulse-height spectrum for $(\mu^-{}^4\text{He})^+$ in 0.8 atm He for a 250-ns time window associated with a muon stop. Detector: Ge. The positions of the Lyman lines are also shown.

IV. CONCLUSIONS

The results of our measurement[36] of the yields of prompt Lyman lines in H_2 are in general agreement with the results of other similar experiments and with the general theoretical picture of the formation and cascade of $\mu^- p$ in gases. In particular they imply that about 7.5% of the $\mu^- p$ stopping in H_2 at 0.8 atm form the $2S$ state of $\mu^- p$.

However, we observed[37] no delayed Lyman K_α x rays, and this implies that less than a few per cent of the $\mu^- p(2S)$ have lifetimes between 50 and 1000 ns. The most likely explanation appears to be that the $\mu^- p(2S)$ atoms are formed dominantly with kinetic energies greater than 0.3 eV, due to chemical or nonradiative Stark processes, and hence are collisionally quenched in times less than 50 ns due to inelastic $2S - 2P$ collisions.

TABLE IV. Summary of muonic helium measurements.

Experiment	Detector	Density	$K_\alpha/K_{\text{total}}$	K_β/K_{total}
SREL, 1967 [a]	Si(Li)	liquid	0.54 ± 0.05	≲0.30
CERN, 1971 [b]	PWC	7 atm	0.62 ± 0.08	≲0.20
CERN, 1974 [c]	Si(Li)	liquid	0.60 ± 0.04	0.32 ± 0.03
This work	Ge	0.8 atm	0.76 ± 0.04	0.04 ± 0.02
LAMPF, 1977				

[a] Reference 26.
[b] Reference 25.
[c] Reference 27.

This argument is somewhat inconsistent with the (admittedly imprecise and indirect) experimental and theoretical information about the $\mu^- p$ velocity distribution obtained in diffusion experiments and with the theoretical values for quenching cross sections.

The absence of long-lived $\mu^- p(2S)$ atoms for H_2 densities of about 1 atm is of course discouraging to plans for laser spectroscopy measurements of the fine structure of the $n=2$ state. It does seem clear that a better understanding of the collisional processes involving $\mu^- p$ in H_2 gas would be useful, and in particular a knowledge of the kinetic energy distribution of $\mu^- p(2S)$. Use of transfer collisions to higher Z atoms might be useful. A substantial improvement in the time or energy resolution of x-ray detectors would, of course, allow an improved experiment of the type reported here to be done.

ACKNOWLEDGMENTS

We are grateful to Dr. Louis Rosen and the staff of LAMPF for their encouragement and support of this experiment. We also thank Mr. L. Trudell for his skillful technical contributions, particularly to the construction of the PWC's, and Mr. C. Grassl for his help with the data analysis. This research was supported in part by the Department of Energy under Contract No. DE-AC02-76ERO 3075. One of the authors (J.V.) would like to thank the Max Kade Foundation for a fellowship.

---

*Present address: Brookhaven National Laboratory, Upton, N. Y. 11973.

[1]DiGiacomo, Nucl. Phys. B 11, 411 (1969); 23, 641(E) (1970).
[2]E. Campani, Lett. Nuovo Cimento 4, 512 (1970).
[3]E. Borie, Z. Phys. A 275, 347 (1975).
[4]E. Borie, Z. Phys. A 278, 127 (1976).
[5]G. Carboni *et al.*, Nucl. Phys. A 278, 381 (1977); Nuovo Cimento A 34, 493 (1976); and A. Bertin *et al.*, Phys. Lett. B 55, 411 (1975).
[6]V. W. Hughes and T. Kinoshaita, *Muon Physics I*, edited by V.W. Hughes and C. S. Wu (Academic, New York, 1977), p. 12.
[7]E. Zavattini, *Proceedings of the Seventh International Conference on High Energy Physics and Nuclear Structures*, edited by M. P. Locher (Birkhäuser, Basel, 1977), p. 49.
[8]A. De Rújula *et al.*, Phys. Lett. B 33, 605 (1970).
[9]H. A. Bethe and E. E. Salpeter, *Quantum Electrodynamics of One- and Two-Electron Atoms* (Springer, Berlin, 1957).
[10]J. Shapiro and G. Breit, Phys. Rev. 113, 179 (1959).
[11]A. S. Wightman, Phys. Rev. 77, 521 (1950); Ph. D. thesis, Princton University, 1949 (unpublished).
[12]M. Leon and H. A. Bethe, Phys. Rev. 127, 636 (1962).
[13]A. Bertin *et al.*, Riv. Nuovo Cimento 5, 423 (1975).
[14]S. S. Gershtein and L. I. Ponomarev, *Muon Physics III*, edited by V. W. Hughes and C. S. Wu (Academic, New York, 1975), p. 141.
[15]G. Kodosky and M. Leon, Nuovo Cimento B 1, 41 (1971).
[16]G. Carboni and G. Fiorentini, Nuovo Cimento B 39, 281 (1977).
[17]R. O. Mueller *et al.*, Phys. Rev. A 11, 1175 (1975).
[18]L. Bracci and G. Fiorentini, Nuovo Cimento A 43, 9 (1978).
[19]A. Alberigi-Quaranta *et al.*, Nuovo Cimento B 47, 92 (1967).
[20]A. Bertin, *Exotic Atoms '79*, edited by K. Crowe *et al.* (Plenum, New York, 1980), p. 161.
[21]H. Anderhub *et al.*, Phys. Lett. B 71, 443 (1977).
[22]F. Kottmann, *Exotic Atoms*, edited by G. Fiorentini and G. Torelli (Laboratori de Frascati, 1977), p. 129.
[23]A. Placci *et al.*, Phys. Lett. B 32, 413 (1970).
[24]B. Budick *et al.*, Phys. Lett. B 34, 539 (1971).
[25]A. Placci *et al.*, Nuovo Cimento A 1, 445 (1971).
[26]R. J. Wetmore *et al.*, Phys. Rev. Lett. 19, 1003 (1967).
[27]G. Backenstoss *et al.*, Nucl. Phys. A 232, 519 (1974).
[28]P. A. Thompson *et al.*, Nucl. Instrum. Methods 161, 391 (1979).
[29]R. D. Stambaugh, Ph. D. thesis, Yale University, 1974 (unpublished); D. E. Casperson *et al.*, Phys. Rev. Lett. 38, 956 (1977).
[30]A. Placci *et al.*, Nuovo Cimento A 64, 1053 (1969).
[31]M. Leon, Phys. Lett. B 35, 413 (1971).
[32]E. Borie and M. Leon, Phys. Rev. A 21, 1460 (1980).
[33]A. Bertin *et al.*, Lett. Nuovo Cimento 18, 277 (1977).
[34]G. Fiorentini and G. Torelli, Nuovo Cimento A 36, 317 (1976).
[35]G. Rinker, Phys. Rev. A 14, 18 (1976).
[36]D. C. Lu *et al.*, Abstracts of Contributed Papers to the Eighth International Conference on High Energy Physics and Nuclear Structure (Vancouver, 1979), p. 14.
[37]P. O. Egan *et al.*, Abstracts of Contributed Papers to the Eighth International Conference on High Energy Physics and Nuclear Structure (Vancouver, 1979), p. 12; P. O. Egan *et al.*, Bull. Am. Phys. Soc. 23, 577 (1978).